Characterisation, analysis and optical properties of nanostructure ZnO using the sol–gel method

M. Kashif[1], Y. Al-Douri[1], U. Hashim[1], M.E. Ali[1], S.M.U. Ali[2,3], M. Willander[2]

[1]*Institute of Nano Electronic Engineering, University Malaysia Perlis, 01000 Kangar, Perlis, Malaysia*
[2]*Physical Electronics and Nanotechnology Division, Department of Science and Technology, Campus Norrkoping, Linkoping University, SE-60174 Norrkoping, Sweden*
[3]*Department of Electronic Engineering, NED University of Engineering and Technology, Karachi 75270, Pakistan*
E-mail: yaldouri@yahoo.com

Published in Micro & Nano Letters; Received on 1st December 2011; Revised on 17th January 2012

Nanostructure ZnO was grown on thin aluminium layer, deposited on silicon substrate using the sol–gel method. The surface morphologies of nanostructure ZnO at different precursor concentrations were studied using scanning electron microscopy. Raman spectroscopy suggested that nanorods started to grow along with nanoflakes at a precursor concentration of 50 mM and the density of the nanorods significantly increases when the concentration was raised to 75 mM. Raman spectra were intensified and red shifted with the increment of precursor concentration. Optical properties of refractive index and optical dielectric constant are investigated. The structural defects at lower level of precursor were probably due to the hypoxic environment, whereas the red shift of Raman spectra was due to the structural change of ZnO nanocrystals.

1. Introduction: Theoretical and experimental efforts have been made to understand the fundamental properties of II–VI semiconductors. The most promising candidates for light-emitting, laser diodes and sensors are II–VI-based materials [1–3].

Nanostructure ZnO are increasingly being used in light-emitting diodes [4], chemical sensors [5], hydrogen storage [6], gas sensors such as hydrogen sensor [7], acetone sensor [8], ethanol sensor [9] etc. because of their unique physical properties. They also exhibit different morphologies in one dimension, such as nanorods, nanotubes, nanobelt and nanoneedles [10–13]. Two-dimensional (2D) ZnO nanostructures, such as nanosheets, nanoplates, nanowalls and nanoporous [14–17], have high surface-to-volume ratios, making them useful for a variety of applications, such as catalysts, nanosieve filters and gas sensors [18].

Different methods have been used to fabricate nanostructure ZnO such as thermal evaporation based on vapour–liquid–solid using metal catalysts or ZnO thin-film catalysts [19], metal organic chemical vapour deposition without catalysts [20], plasma-assisted molecular beam epitaxy [21] and hydrothermal method [22].

In this work, ZnO nanoflakes were fabricated via the sol–gel technique at different precursor concentrations (12.5–75 mM). The morphology of the ZnO nanoflakes was characterised using scanning electron microscopy (SEM).The optical properties and structural integrity of the ZnO nanoflakes were investigated using Raman spectroscopy. Although higher precursor concentration improved the formation of nanorods and crystal quality of ZnO, it inflicted intrinsic defects on the fabricated nanostructures, probably by creating a hypoxic atmosphere at the elevated level of precursor.

2. Experimental part: The p-type silicon (Si) wafer (100) was used as a substrate for the growth of n-type nanostructure ZnO. Si substrates (1 × 1.5 cm) were cleaned in acetone, ethanol and deionised (DI) water using ultrasonic cleaner followed by buffered oxide etch (BOE) cleaning to remove the native oxide layer. A very thin aluminium (Al) layer (~25 nm) was deposited on Si substrate using thermal evaporator. ZnO nanoflakes were grown on Al-coated Si substrate by the hydrothermal method [22]. To prepare the seed solution, 2-methoxyethanolamine was dissolved in 0.35 M of zinc acetate dehydrate solution under vigorous stirring for 30 min. Then monoethanolamine was added to the solution dropwise under constant stirring at 60°C for 2 h until it became transparent and homogenous. The resultant solution was spin coated on Si substrate at 3000 rpm for 20 s. The substrates were then dried on hot plate at 250°C for 15 min to remove the organic impurities. The coating and drying process was repeated for three times.

ZnO nanoflakes were grown on seeded Al–Si substrate using variable concentrations (12.5–75 mM) of precursors [zinc nitrate hexahydrate and hexamethyl tetra-amine (HMT) solution] in 150 ml DI water. The substrate was placed in a downward facing sample holder made up of Teflon and was incubated in a preheated oven at 93°C for 2 h. Subsequently, ZnO nanoflakes were washed with DI water and dried with N_2 gun.

The morphological characterisations of ZnO nanoflakes were performed using a SEM (JEOL JSM6460LA). The optical properties and structural qualities were studied with Raman spectroscopy (Jobin Yvon Horiba HR800UV) system and X-ray diffraction (XRD, Philips PW 1710 X-ray diffractometer), respectively.

3. Results and discussion: Previously, Al has been used as a substrate to form the porous structure of ZnO nanoplates [15, 22]. While Al facilitates the formation of porous structure by inhibiting the growth of nanorods [22, 23], using Al as a substrate to grow ZnO porous structures have some potential problems: (i) Al is quickly oxidised by atmospheric oxygen, (ii) removal of Al-oxide cannot be readily done without destroying the structural integrity of the substrate, and (iii) Al is a good conductor and therefore a thick layer of Al under the nanostructure ZnO might be problematic while applying in electrical devices. On the other hand, Si is a semiconductor substrate and easily available at cheaper prices. The oxide layer of Si substrate can be easily removed by diluted hydrofluoric acid without destroying its structural integrity. In the present study, ZnO nanoflakes are grown on a thin layer (25 nm) of Al deposited on Si substrate. The thin Al layer is dissolved into $Al(OH)_4$ in the alkaline environment of HMT and 2D ZnO originates from its anisotropic structure. The additive $Al(OH)_4$ ions play a regulatory function that promotes the formation of porous structure and inhibits the formation of nanorods [22]. Thus, the use of a thin layer of Al totally eliminated the negative impacts of Al substrate.

Fig. 1 shows the effect of precursor concentration on the nanostructure ZnO morphologies. A uniform distribution of the nanoflakes on the Si substrate was observed when the growth was completed with a 12.5 mM precursor (Fig. 1*a*). The SEM image revealed a wall thickness of 80–100 nm and a diameter of

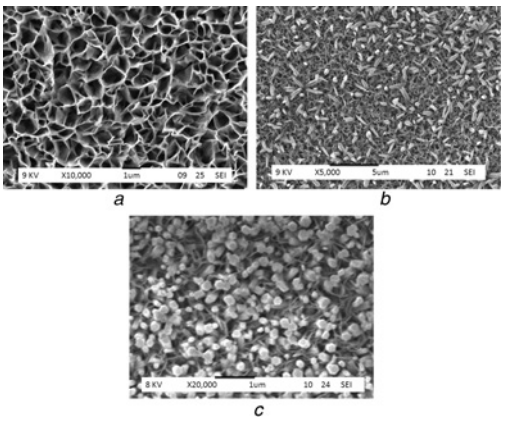

Figure 1 *SEM images of ZnO nanoflakes showing surface morphology of precursor*
a 12.5 mM
b 50 mM
c 75 mM

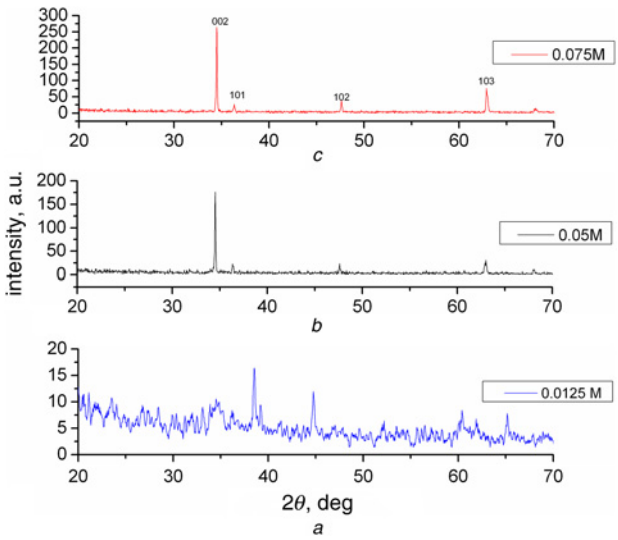

Figure 2 *XRD patterns of ZnO nanoflakes of precursor*
a 12.5 mM
b 50 mM
c 75 mM

300–500 nm of the grown nanoflakes. When the precursor's concentration was raised to 50 mM, growth of ZnO nanorods was observed on the surface and walls of the nanoflakes (Fig. 1*b*). The density of the nanorods was increased and the length was decreased when the precursor concentration was further raised to 75 mM (Fig. 1*c*) [24]. Surprisingly, the entire surface of the nanoflakes was occupied by small hexagonal nanorods that apparently appeared as granules, probably owing to the reduction of length (Fig. 1*c*). This reflects a great role of precursor on the morphological features of nanoflakes and nanorods.

The exact mechanisms of structural transition from nanoflakes to nanorods are not clearly described in earlier studies. It has been implicated that the relaxation of lattice-mismatch-induced strain has a great role in the initial phase of nanostructure growth [23]. However, this cannot be the causative factor in the present case as Al favours the growth of sheet-like structure and inhibits the formation of nanorods or nanowires by capping the growing ZnO surface [22]. The preferred growth of nanorods may be correlated with the fact that the density of dangling bonds at the crossing points or the end of nanowalls is higher than that at other positions. The concentration of these bonds leads to the accumulation of adatoms or molecules to maintain a low level of energy in the whole system, and then nanorods are formed in the succeeding growth [23], where concentration-dependent surface stress or atomic deposition on the surface derives phase refining. As a result of the competition between these two effects, the phases sometimes select stable, nanometric or sizes [25]. The XRD pattern of nanostructure ZnO with different precursor concentrations is shown in Fig. 2. All the peaks in the pattern correspond to hexagonal structure of ZnO. Significant changes have shown an increase of peak intensity corresponding to (002) crystal plane with increasing of precursor concentration. However, at lower precursor concentration of 12.5 mM, there are two distinct peaks around 39° and 45° that are most probably because of the thin Al layer. It was observed that at lower concentration, the thin Al layer is not fully dissolved with the nanostructure ZnO as compared to higher concentrations. Previously, the researchers [15, 22] have been used Al as a substrate and the peaks at lower precursor concentration; 39° and 45° are in accordance with these results.

Raman spectroscopy can provide useful information about the qualities of crystals and structures of ZnO nanoflakes and nanorods. The operating principles and theoretical background of Raman data interpretation can be found elsewhere [26]. Fig. 3 shows the Raman scattering spectra of the ZnO nanoflakes produced by the sol–gel method in the current study. The spectra were collected by exciting a laser line at 488 nm with excitation power of 20 mW. One sharp peak at 520 cm^{-1} and two weak peaks at 300 and 615 cm^{-1} (Fig. 3*a*) can be conferred to the TO phonon mode originating from Si substrate [26]. When the depth of light penetration exceeds product thickness, such peaks might appear [27]. Thus, they were not affected by precursor concentration and could not provide useful information about the qualities of ZnO. The peak that appeared at 433 cm^{-1} with significantly high intensity is a typical characteristic of hexagonal wurtzite ZnO. The intensity of this peak was very low at 12.5 mM precursor but drastically intensified with the increment of precursor level (green and blue dotted line). This peak was assigned to the Raman active optical phonon of E_{2H} mode [28].

Two weak peaks that appeared at 330 and 380 cm^{-1} were assigned to multi-phonon scattering process (E_{2H}–E_{2L}) and A_1T mode, respectively [29]. They were totally absent at 12.5 mM precursor, became clearly visible at 75 mM precursor, clearly showing the influence of precursor concentration in the synthesis of ZnO nanoflakes. The magnified view of the Raman spectra between (400 and 480 cm^{-1}) window is shown in (Fig. 3*b*). It was observed that the peak position of E_{2H} mode shifts 4 cm^{-1} from 429 to 433 cm^{-1} when the precursor concentration was raised to 50 and 75 mM. The optical energy bandgaps (E_g) of nanostructure ZnO are calculated from photoluminescence spectroscopy (results not shown here) using the relation

$$E_g = hc/\lambda \tag{1}$$

where E_g is the energy gap, h is the Planck constant, c is the speed of light and λ is the wavelength. The calculated values are 3.2191, 3.2375 and 3.37 eV for precursor concentration of 12.5, 50 and 75 mM, respectively.

Many attempts have been made to relate the refractive index and the energy gap E_g through simple relationships [30–35]. However, these relations of n are independent of temperature and incident photon energy. Here the various relations between n and E_g will be reviewed. Ravindra *et al.* [35] had been presented a linear form of n as a function of E_g

$$n = \alpha + \beta E_g \tag{2}$$

where $\alpha = 4.048$ and $\beta = -0.62\ eV^{-1}$. Light refraction and dispersion will be inspired. Herve and Vandamme [36] proposed an

doi: 10.1049/mnl.2011.0681

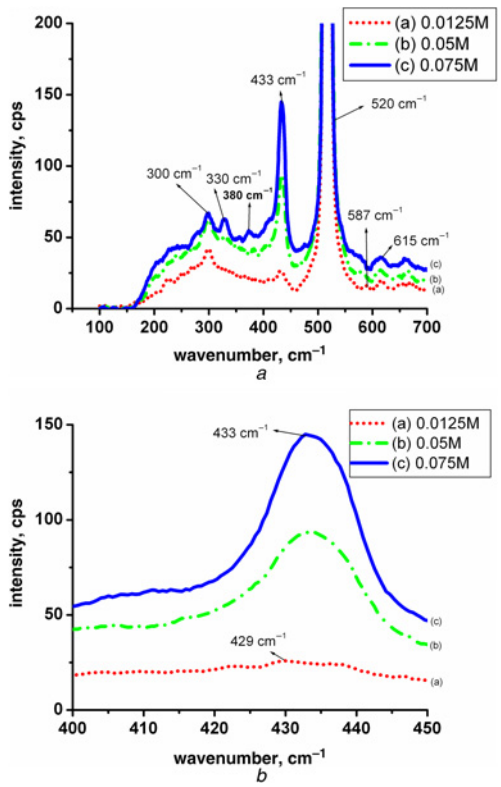

Figure 3 *Raman spectrum of ZnO nanoflakes*
a Between 100 and 700 cm^{-1}
b Magnified view showing the Raman shift near 430 nm region

empirical relation as follows

$$n = \sqrt{1 + \left(\frac{A}{E_g + B}\right)^2} \tag{3}$$

where $A = 13.6$ eV and $B = 3.4$ eV. For group-IV semiconductors, Ghosh *et al.* [37] have published an empirical relationship based on the band structure and quantum dielectric considerations of Penn [38] and Van Vechten [39]

$$n^2 - 1 = \frac{A}{(E_g + B)^2} \tag{4}$$

where $A = 8.2E_g + 134$, $B = 0.225E_g + 2.25$ and $(E_g + B)$ refers to an appropriate average energy gap of the material. The calculated refractive indices of the end-point compounds and energy gaps are listed in Table 1, and give good agreement with experimental [40, 41] and theoretical [42–45] values.

This is verified by the calculation of the optical dielectric constant ε_∞ which depends on the refractive index. Note that the optical dielectric constant $\varepsilon_\infty = n^2$ [46]. It is clear that the investigated refractive indices n using model of Ravindra *et al.* [35] is important for nanostructure ZnO in enhancing the detecting and sensing. It means high absorption may be attributed to increase sensors efficiency.

There was a significant change in surface morphology nanostructure ZnO during a transition from nanoflakes to nanorods. The tubular-shaped nanoflakes walls (Fig. 1*a*) behaved as resonant cavities and change the structure [47] causing red shift in Raman spectra [48].

We found the morphologies of ZnO nanoflakes (Fig. 1*a*) similar to the tubular shapes of ZnO nanotubes. The walls of the nanoflakes most likely behave as resonant cavities owing to structural change [47].

We identified the appearance of 587 cm^{-1} LO phonon peak that is indicative of oxygen crisis at lower precursor (25 mM) (Fig. 3*a*) was in good agreement with the theoretical model [49]. At high precursor concentration (75 mM) such peak cannot be observed, indicating very low level of intrinsic defects owing to oxygen crisis. As identical excitation energy of laser power was used in all measurements, the disappearance of LO phonon peak cannot be referred to the thermal destruction of ZnO nanocrystal. Higher intensities of E_{2H} phonon than LO phonon mode are suggestive of little defects in ZnO nanocrystals [50]. Fig. 3*a* clearly shows that at high concentration (75 mM) of precursor E_{2H} phonon at 433 cm^{-1} is intensified and LO phonon at 587 cm^{-1} completely disappeared. This clearly reflects better quality of ZnO nanocrystal in the developed nanoflakes.

We successfully demonstrated that with a change in precursor concentration, ZnO nanoflakes of different morphological features can be realised and the morphological features have significant effects on the optical properties.

4. Conclusions: The effects of precursor concentration on the morphological, optical and crystalline properties of nanostructure ZnO were studied. It was found that precursor concentration plays a vital role in the transition of nanoflakes to nanorods. At low precursor concentration nanoflakes configuration dominated. However, nanoflakes surfaces were covered with the protruding nanorods when concentration was raised. Raman scattering studies reflected improved crystal qualities and reduced structural defects at a higher level of precursor. The red shifting of Raman spectra were

Table 1 Energy gaps, calculated refractive indices of nanostructure ZnO using Herve and Vandamme [34], Ravindra *et al.* [35] and Ghosh *et al.* [36] models corresponding to optical dielectric constant

Concentration, mM	Energy, eV	*n*	ε_∞
12.5	3.2191 3.44[a] 1.57[b] 0.73[c] 0.88[d] 2.26[e]	2.052[f] 2.285[g] 2.276[h] 2.008[i]	4.210[f] 5.221 [g] 5.180[h]
50	3.2375	2.040[f] 2.279[g] 2.270[h]	4.161[f] 5.193[g] 5.152[h]
75	3.37	1.954[f] 2.244[g] 2.230[h]	3.833[f] 5.035[g] 4.973[h]

[a]Hummer [40] – Exp.
[b]Charifi *et al.* [42] – Theor.
[c]Schleife *et al.* [43] – Theor.
[d]Xu and Ching [44] – Theor.
[e]Schroer *et al.* [45] – Theor.
[f]Ravindra *et al.* [35].
[g]Herve and Vandamme [36].
[h]Ghosh *et al.* [37].
[i][41] – Exp.

attributed to the structural change from ZnO nanoflakes to nanorods. The optical properties are investigated and proved that Ravindra *et al.* model especially with increasing precursor concentrations is more appropriate for nanostructure ZnO applicable in sensors.

5. Acknowledgments: This work has been achieved using FRGS grant 9003−00249 and 9003-00255. The author (Y.Al-Douri) would like to acknowledge TWAS, Italy for full support of his visit to JUST – Jordan under TWAS-UNESCO Associateship.

6 References

[1] Gunshor R.L., Nur?mikko A.V., Otsuka N.: 'The molecular beam epitaxial growth of wide gap II−VI injection lasers and light-emitting diodes', *Thin Solid Films*, 1993, **231**, p. 190

[2] Nurmikko A.V., Gunshor R.L.: 'Optical physics and laser devices in II−VI quantum confined heterostructures', *Physica B*, 1993, **185**, p. 16

[3] Al-Douri Y.: 'Electronic and optical properties of $Zn_xCd_{1-x}Se$', *Mater. Chem. Phys.*, 2003, **82**, p. 49

[4] Guo H., Lin Z., Feng Z., Lin L., Zhou J.: 'White-light-emitting diode based on ZnO nanotubes', *J. Phys. Chem. C*, 2009, **113**, p. 12546

[5] Umar A., Rahman M.M., Kim S.H., Hahn Y.-B.: 'Zinc oxide nanonail based chemical sensor for hydrazine detection', *Chem. Commun.*, 2008, **2**, p. 166

[6] Wan Q., Lin C.L., Yu X.B., Wang T.H.: 'Room-temperature hydrogen storage characteristics of ZnO nanowires', *Appl. Phys. Lett.*, 2004, **84**, p. 124

[7] Mridha S., Basak D.: 'Investigation of a p-CuO/n-ZnO thin film heterojunction for H_2 gas-sensor applications', *Semicond. Sci. Technol.*, 2006, **21**, p. 928

[8] Zeng Y., Zhang T., Yuan M., *ET AL.*: 'Growth and selective acetone detection based on ZnO nanorod arrays', *Sens. Actuators B, Chem.*, 2009, **143**, p. 93

[9] Yang Z., Li L.-M., Wan Q., Liu Q.-H., Wang T.-H.: 'High-performance ethanol sensing based on an aligned assembly of ZnO nanorods', *Sens. Actuators B, Chem.*, 2008, **135**, p. 57

[10] Manekkathodi A., Lu M.-Y., Wang C.W., Chen L.-J.: 'Direct growth of aligned zinc oxide nanorods on paper substrates for low-cost flexible electronics', *Adv. Mater.*, 2010, **22**, p. 4059

[11] Xi Y., Song J., Xu S., *ET AL.*: 'Growth of ZnO nanotube arrays and nanotube based piezoelectric nanogenerators', *J. Mater. Chem.*, 2009, **19**, p. 9260

[12] Cao B.Q., Liu Z.M., Xu H.Y., *ET AL.*: 'Catalyst/dopant-free growth of ZnO nanobelts with different optical properties from nanowires grown via a catalyst-assisted method', *Cryst. Eng. Commun*, 2011, **13**, p. 4282

[13] Cho S., Lee K.-H.: 'Synthesis of ZnO nanostructures composed of nanosheets with controllable morphologies', *Cryst. Growth Des.*, 2009, **10**, p. 1289

[14] Wang N., Jiang L., Peng H., Li G.: 'Synthesis of ZnO nanostructures composed of nanosheets with controllable morphologies', *Cryst. Res. Technol.*, 2009, **44**, p. 341

[15] Cheng J.P., Liao Z.M., Shi D., Liu F., Zhang X.B.: 'Oriented ZnO nanoplates on Al substrate by solution growth technique', *J. Alloys Compd.*, 2009, **480**, p. 741

[16] Mäder M., Gerlach J.W., Höche T., *ET AL.*: 'ZnO nanowall networks grown on DiMPLA pre-patterned thin gold films', *Phys. Status Solidi-Rapid Res. Lett.*, 2008, **2**, p. 200

[17] Kashif M., Ali S.M.U., Foo K.L., Hashim U., Willander M.: 'ZnO nanoporous structure growth, optical and structural characterization by aqueous solution route'. Enabling Science and Nanotechnology Int. Conf. (EsciNano), (AIP Conf. Proc.), Kuala Lumpur, Malaysia, 2010, vol. 92, p. 1341

[18] Chang J.F., Kuo H.H., Leu I.C., Hon M.H.: 'The effects of thickness and operation temperature on ZnO:Al thin film CO gas sensor', *Sens. Actuators B, Chem.*, 2002, **84**, p. 258

[19] Kim S.-W., Park H.-K., Yi M.-S., *ET AL.*: 'Epitaxial growth of ZnO nanowall networks on GaN/sapphire substrates', *Appl. Phys. Lett.*, 2007, **90**, article id. 033107

[20] Lee W., Jeong M.-C., Myoung J.-M.: 'Catalyst-free growth of ZnO nanowires by metal organic chemical vapour deposition (MOCVD) and thermal evaporation', *Acta Mater.*, 2004, **52**, p. 3949

[21] Su S.C., Lu Y.M., Zhang Z.Z., *ET AL.*: 'Structural, optical, and hydrogenation properties of ZnO nanowall networks grown on a Si (111) substrate by plasma-assisted molecular beam epitaxy', *Physica B*, 2008, **403**, p. 2590

[22] Cheng J.P., Zhang X.B., Luo Z.Q.: 'Oriented growth of ZnO nanostructures on Si and Al substrates', *Surf. Coat. Technol.*, 2008, **202**, p. 4681

[23] Zhang B.P., Wakatsuki K., Binh N.T., Segawa Y., Usami N.: 'Low-temperature growth of ZnO nanostructure networks', *J. Appl. Phys.*, 2005, **96**, p. 340

[24] Li F., Li Z., Jin F.J.: 'Structural and luminescent properties of ZnO nanorods prepared from aqueous solution', *Mater. Lett.*, 2007, **61**, p. 1876

[25] Walgraef D.: 'Nanostructure initiation during the early stages of thin film growth', *Physica E*, 2002, **15**, p. 33

[26] Willander M., Yang L.L., Wadeasa A., *ET AL.*: 'Zinc oxide nanowires: controlled low temperature growth and some electrochemical and optical nano devices', *J. Mater. Chem.*, 2009, **19**, p. 1006

[27] Zhaochun Z., Baibiao H., Yongqin Y., Deliang C.: 'Electrical properties and Raman spectra of undoped and Al-doped ZnO thin films by metalorganic vapor phase epitaxy', *Mater. Sci. Eng. B, Adv.*, 2001, **86**, p. 109

[28] Xing Y.J., Xi Z.H., Xue Z.Q., *ET AL.*: 'Optical properties of the ZnO nanotubes synthesized via vapor phase growth', *Appl. Phys. Lett.*, 2003, **83**, p. 1689

[29] Fan H.J., Scholz R., Kolb F.M., *ET AL.*: 'On the growth mechanism and optical properties of ZnO multi-layer nanosheets', *Appl. Phys. A, Mater.*, 2004, **79**, p. 1895

[30] Moss T.S.: 'A relationship between the refractive index and the infra-red threshold of sensitivity for photoconductors', *Proc. Phys. Soc. B*, 1950, **63**, p. 167

[31] Gupta V.P., Ravindra N.M.: 'Comments on the Moss formula', *Phys. Status Solidi B*, 1980, **100**, p. 715

[32] Al-Douri Y., Feng Y.P., Huan A.C.H.: 'Optical investigations using ultra-soft pseudopotential calculations of $Si_{0.5}Ge_{0.5}$ alloy', *Solid State Commun.*, 2008, **148**, p. 521

[33] Al-Douri Y., Reshak A.H., Baaziz H., *ET AL.*: 'An ab initio study of the electronic structure and optical properties of $CdS_{1-x}Te_x$ alloys', *Sol. Energy*, 2010, **84**, p. 1979

[34] Herve P., Vandamme L.K.J.: 'General relation between refractive index and energy gap in semiconductors', *Infrared Phys. Technol.*, 1993, **35**, p. 609

[35] Ravindra N.M., Auluck S., Srivastava V.K.: 'On the Penn gap in semiconductors', *Phys. Status Solidi (b)*, 1979, **93**, p. K155

[36] Herve P.J.L., Vandamme L.K.J.: 'Empirical temperature dependence of the refractive index of semiconductors', *J. Appl. Phys.*, 1995, **77**, p. 5476

[37] Ghosh D.K., Samanta L.K., Bhar G.C.: 'A simple model for evaluation of refractive indices of some binary and ternary mixed crystals', *Infrared Phys.*, 1984, **24**, p. 34

[38] Penn D.R.: 'Wave-number-dependent dielectric function of semiconductors', *Phys. Rev.*, 1962, **128**, p. 2093

[39] Van Vechten J.A.: 'Theory of electronegativity in covalent systems. I. Electronic dielectric constant', *Phys. Rev.*, 1969, **182**, p. 891

doi: 10.1049/mnl.2011.0681

[40] Hummer K.: 'Interband magnetoreflection of ZnO', *Phys. Status Solidi (b)*, 1973, **56**, p. 249
[41] Weast R.C. (Ed.): 'Handbook of chemistry & physics' (CRC Press, 1973, 5th edn.)
[42] Charifi Z., Baaziz H., Reshak A.H.: 'Ab-initio investigation of structural, electronic and optical properties for three phases of ZnO compound', *Phys. Status Solidi (b)*, 2007, **244**, p. 3154
[43] Schleife A., Fuchs F., Furthmuller J., Bechstedt F.: 'First-principles study of ground- and excited-state properties of MgO, ZnO, and CdO polymorphs', *Phys. Rev. B*, 2006, **73**, article id. 245212
[44] Xu Y.-N., Ching W.Y.: 'Electronic, optical, and structural properties of some wurtzite crystals', *Phys. Rev. B*, 1993, **48**, p. 4335
[45] Schroer P., Kruger P., Pollmann J.: 'First-principles calculation of the electronic structure of the wurtzite semiconductors ZnO and ZnS', *Phys. Rev. B*, 1993, **47**, p. 6971
[46] Samara G.A.: 'Température and pressure dépendances of the dielectric constants of semiconductors', *Phys. Rev. B*, 1983, **27**, p. 3494
[47] Israr M.Q., Sadaf J.R., Yang L.L., *ET AL.*: 'Trimming of aqueous chemically grown ZnO nanorods into ZnO nanotubes and their comparative optical properties', *Appl. Phys. Lett.*, 2009, **95**, article id. 073114
[48] Yang R.D., Tripathy S., Li Y., Sue H.-J.: 'Photoluminescence and micro-Raman scattering in ZnO nanoparticles: the influence of acetate adsorption', *Chem. Phys. Lett.*, 2005, **411**, p. 50
[49] Fonoberov V.A., Balandin A.A.: 'Interface and confined optical phonons in wurtzite nanocrystals', *Phys. Rev. B*, 2004, **70**, article id. 233205
[50] Abdulgafour H.I., Hassan Z., Al-Hardan N., Yam F.K.: 'Growth of zinc oxide Nanoflowers by thermal evaporation method', *Physica B*, 2010, **405**, p. 2570